Quantified Binding Scale of Competing Ligands at the Surface of Gold Nanoparticles: The Role of Entropy and Intermolecular Forces

*Claire Goldmann, François Ribot, Leonardo F. Peiretti, Paola Quaino, Frederik Tielens, Clément Sanchez, Corinne Chanéac, and David Portehault**

***A** basic understanding of the driving forces for the formation of multiligand coronas or self-assembled monolayers over metal nanoparticles is mandatory to control and predict the properties of ligand-protected nanoparticles. Herein, ^{1}H nuclear magnetic resonance experiments and advanced density functional theory (DFT) modeling are combined to highlight the key parameters defining the efficiency of ligand exchange on dispersed gold nanoparticles. The compositions of the surface and of the liquid reaction medium are quantitatively correlated for bifunctional gold nanoparticles protected by a range of competing thiols, including an alkylthiol, arylthiols of varying chain length, thiols functionalized by ethyleneglycol units, and amide groups. These partitions are used to build scales that quantify the ability of a ligand to exchange dodecanethiol. Such scales can be used to target a specific surface composition by choosing the right exchange conditions (ligand ratio, concentrations, and particle size). In the specific case of arylthiols, the exchange ability scale is exploited with the help of DFT modeling to unveil the roles of intermolecular forces and entropic effects in driving ligand exchange. It is finally suggested that similar considerations may apply to other ligands and to direct biligand synthesis.*

1. Introduction

Surface functionalization is a pillar of modern colloidal science focusing on nanostructures. For instance, using organic molecules as surface complexing agents, so-called ligands, on gold nanoparticles allows introducing and managing functionality in application fields such as sensors[1] or biomedicine.[2–4] Such capping agents can also be adequately chosen and introduced during colloidal synthesis to control the growth of nanoparticles and to tune their size, shape, and dispersion state.[5–7] In most cases, the ligand shell or self-assembled monolayer (SAM) is actually constituted of several ligands so as to provide multifunctionality[4,8–11] or to ensure functionalization by given moieties,[12,13] while other ligands with simple hydrophobic or hydrophilic chains provide colloidal stability in organic or aqueous media, respectively.

Bifunctional nanoparticles can be obtained by two methods: ligand exchange, where particles first synthesized with ligands A only are processed in solution to exchange a fraction of A by ligands B (**Figure 1**a); and biligand synthesis, where the particles are directly synthesized in contact with ligands A and B (Figure 1b).

In both cases, the main difficulty is to control the final composition of the ligand shell. In order to understand,[10,14–17]

Dr. C. Goldmann, Dr. F. Ribot, Dr. F. Tielens, Prof. C. Sanchez, Dr. C. Chanéac, Dr. D. Portehault
Laboratoire de Chimie de la Matière Condensée de Paris (CMCP)
Sorbonne
Universités-UPMC Univ Paris 06
CNRS
Collège de France
4 Place Jussieu 75005 Paris, France
E-mail: david.portehault@upmc.fr
Dr. L. F. Peiretti, Dr. P. Quaino
Preline, Facultad de Ingeniería Química
Universidad Nacional del Litoral
3000 Santa Fe, Argentina

DOI: 10.1002/smll.201604028

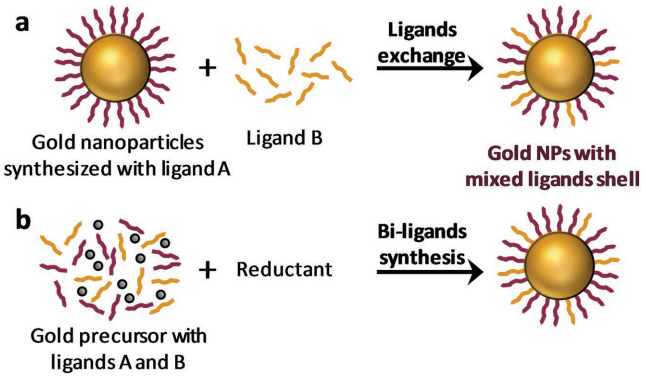

Figure 1. The two pathways used to obtain nanoparticles with a mixed ligand shell: a) ligand exchange and b) biligand synthesis.

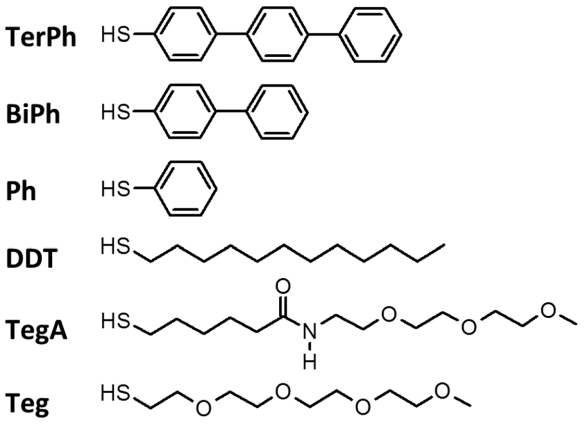

Figure 2. Molecular structures of the ligands used in this study.

control,[18] and predict[19] the properties of such very common, yet complex, hybrid nanoparticles made of an inorganic core and a bicomponent organic corona, the composition of the shell must be assessed. Various methods can unveil the composition of biligand shells, such as mass spectrometries,[20,21] electron paramagnetic resonance,[22] fluorescence,[4,23] and surface enhanced Raman spectroscopies.[24] Liquid state Nuclear Magnetic Resonance (NMR) is also a versatile tool to quantify the ligand shell composition for a range of molecules and inorganic cores,[25–29] to study the ligand surface distribution,[25,29–32] and the exchange dynamics.[33–36] Among these state-of-the art studies, only a few correlate together the shell and medium compositions at the steady state[24,26,37] or during the exchange process.[35,36]

Extending to other ligands and particle sizes, quantification at the steady state of the molecular partition between mixed ligand shells and the surrounding medium should provide two significant advances. First, quantified partition could be used to predict the composition of the mixed SAM for a given ligand ratio in the initial solution, and even to select the right initial ratio to reach a targeted surface composition. Second, and more fundamentally, quantifying the partition for a series of well-chosen ligands should provide new insights into the role of the chain length and functionality,[16,17,19,38–44] and of the end-group[28,29,45,46] on ligand exchange and the stability of mixed ligand shells. In brief, such quantified partitions may contribute to decipher the impact of intermolecular forces and entropic effects on the stability of the ligand shells and their role as driving forces for ligand exchange—a topical issue for the control of nanoparticles properties and self-assembly.[4,8–13,41,47–49]

Herein, we focus on the influence of the ligand molecular structure on the final surface composition of ligand-capped gold nanoparticles. We use NMR to investigate ligand exchange for a range of thiol ligands, and build quantitative scales of molecular partition as a measure of the exchange ability for each ligand. We especially investigate a series of arylthiols by coupling experiments with density functional theory (DFT) modeling, in order to interpret, in depth, the molecular principles underlying ligand exchange for these molecules. We investigate, in depth, the prime importance of intermolecular chain interactions in the stabilization and composition of mixed ligand shells on nanoparticles, and shed new light on the role of entropic effects. We then extend the approach to other ligands and to biligand syntheses.

2. Results and Discussion

The thiol ligands used in this study (**Figure 2**) differ by the functionalities of their chain. Dodecanethiol (DDT) contains only CH_2 units. Ph, BiPh, and TerPh contain 1, 2, and 3 aromatic phenyl groups, respectively. In a second step, two ligands (TegA and Teg) containing several ethyleneglycol units are investigated. The TegA ligand contains also an alkyl spacer and an amide function. Each ligand provides different preponderant intermolecular forces, originating from dispersion, van der Waals or dipolar interactions, H-bonding or π-stacking.

2.1. Determination of the Surface Composition: The Case Study of Dodecanethiol/*p*-Terphenylthiol Mixed Ligand Corona

When a ligand is grafted onto the surface of a nanoparticle, its NMR signals are broadened because of the distribution of local environments, which spread the associated chemical shifts, and because of shorter transverse relaxation times, which arise from a decrease of its rotational mobility (degrees of freedom).[50] This broadening, which increases with the proximity of the surface, can be so important that the signal completely flattens out in the baseline,[51,52] as observed for the CH_2S moieties, the closest to the surface in aliphatic thiol-stabilized gold particles.[53] On the contrary, free ligands yield sharp NMR signals. This difference was used to monitor ligand exchange. **Figure 3** shows portions of the ^{1}H NMR spectra of a suspension of 2-nm DDT-stabilized nanoparticles during exchange with TerPh (full spectra shown in Figure S1, Supporting Information) with a total TerPh proportion of 52 mol%. No particle size evolution was detected by transmission electron microscopy (TEM) (Figure S2, Supporting Information) after 110 h. The sharp signal at 3.50 ppm of the thiol proton of free TerPh (**a′** in Figure 3) appears after the addition of TerPh, and then slowly decreases upon grafting of TerPh. The DDT quadruplet at 2.52 ppm (**b** in Figure 3),

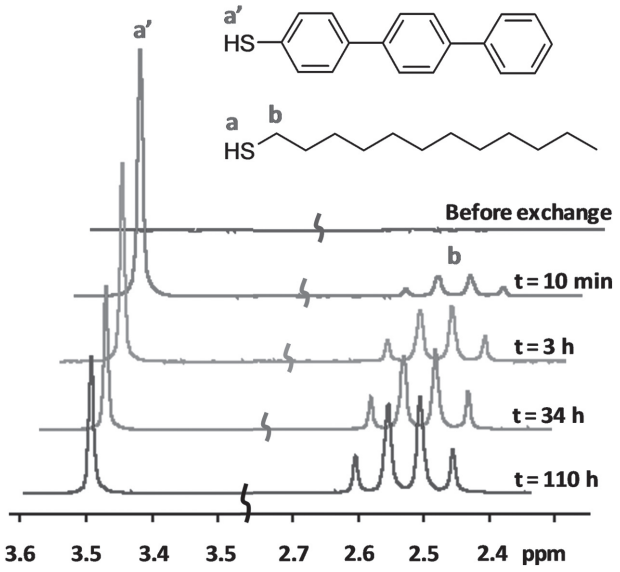

Figure 3. Time evolution of specific ^{1}H NMR signals during the exchange of DDT by TerPh (total TerPh proportion of 52%), in $CDCl_3$, at a nanoparticles concentration of 10^{-4} M for a particle diameter of 2 nm.

corresponding to the α-CH_2 next to the sulfur atom, concomitantly grows immediately after the addition of TerPh.

Upon release of DDT, integration of these signals yields the relative amounts of free ligands. By using the ^{1}H NMR spectrum of a blank solution of known concentration and volume acquired in the same conditions, the integrations are converted in absolute quantities of free species, yielding the time evolution represented in **Figure 4**. Once the ^{1}H NMR spectra do not change anymore (110 h for DDT/TerPh couple), all thiol species are converted into free disulfides with the "iodine death reaction".[54] The total amount of

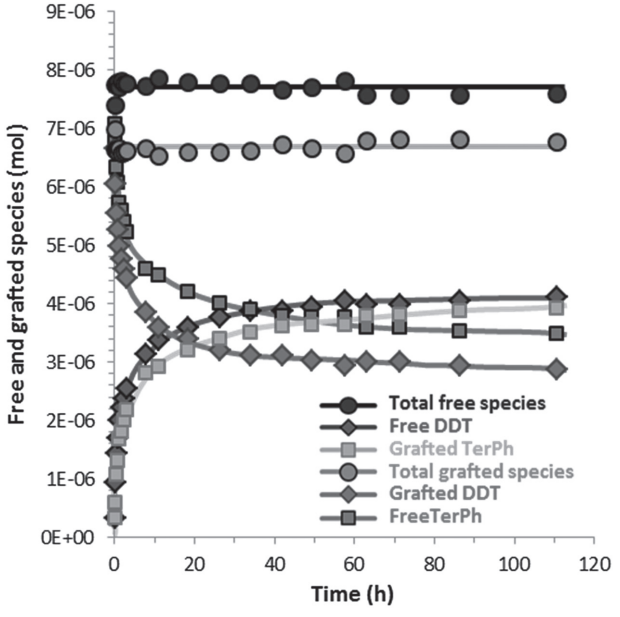

Figure 4. Time evolution of the amounts of each free and grafted species during the exchange of DDT by TerPh (total TerPh proportion of 52%), in $CDCl_3$, at a nanoparticles concentration of 10^{-4} M for a particle diameter of 2 nm.

DDT in the reaction medium (DDT_{total}), which corresponds to the initial quantity of bonded DDT, is determined by integration. The surface composition at a given time is then derived with the following simple relations:

$$DDT_{grafted}(t) = DDT_{total} - DDT_{solution}(t) \quad (1)$$

$$TerPh_{grafted}(t) = TerPh_{added} - TerPh_{solution}(t) \quad (2)$$

$DDT_{solution}(t)$ and $TerPh_{solution}(t)$ being the quantities of free DDT and free TerPh at a given time, respectively. The maximal uncertainty of these quantity measurements was evaluated to ≈2% (see the Supporting Information).

The time evolution of each grafted species at a nanoparticles concentration of 10^{-4} M is reported in Figure 4. The total quantities of grafted and free species remain constant, suggesting that the exchange of DDT by TerPh occurs with a 1:1 stoichiometry, as mentioned in previous works on different thiols.[38] The overall reaction can be written

$$DDT_{surface} + B_{solution} \rightleftarrows DDT_{solution} + B_{surface} \quad (3)$$

In few cases, mostly with the TegA ligand but not with arylthiols, a change in the particle size was evidenced. Accordingly, even if the 1:1 stoichiometry is respected, a slight increase in the quantity of grafted species is observed, in agreement with the increase of gold surface area (Figure S3b, Supporting Information).

The grafting density of the initial DDT monolayer was evaluated from the quantity of grafted ligands and the geometrical surface of the particles. A coverage of about 5 thiols nm^{-2} is obtained, which is consistent with literature[55] and in agreement with the slight variations in particle size observed in the size distributions (Figures S4 and S5, Supporting Information). As the exchange proceeds through a 1:1 stoichiometry, grafting densities are constant and similar in all experiments.

Noteworthy, the same coverage value of ≈5 thiols nm^{-2} and exchange stoichiometry are measured on 2-nm and 5-nm particles for all ligands considered in this study. Furthermore, TEM observations yield similar spherical nanoparticle shapes for all exchange experiments (Figures S4–S6, Supporting Information).

2.2. Partition Ratios: Building the Ligand Exchange Efficiency Scale

The procedure described above was applied to both 2-nm and 5-nm diameter nanoparticles, initially stabilized by DDT. The exchanges were carried out with ligands Ph, BiPh, TerPh, TegA, and Teg added in various amounts. ^{1}H NMR was used to monitor specific signals: CH_2S at 2.52 ppm for DDT; SH at 3.50 ppm for Ph, BiPh, and TerPh; CH_2S at 2.70 ppm for Teg; and CH_2S at 2.54 ppm for TegA. In the latter case, a deconvolution step was necessary to separate free DDT from free TegA.

For a given B species (Ph, BiPh, TerPh, TegA, or Teg), the compositions of the whole reaction medium ($\%B_{medium}$) and

of the nanoparticles surface ($\%B_{surface}$) at the steady state are calculated from the NMR titration curves as follows:

$$\%B_{medium} = 100 \frac{\text{quantity of } B \text{ in solution and grafted}}{\text{quantity of } A \text{ and } B \text{ in solution and grafted}} \quad (4)$$

$$\%B_{surface} = 100 \frac{\text{quantity of } B \text{ grafted}}{\text{quantity of } A \text{ and } B \text{ grafted}} \quad (5)$$

Figure 5a shows a partition diagram for Ph, BiPh, and TerPh, where the surface composition is plotted versus the composition of the whole reaction medium for every ligand couple considered. Apart from few exceptions, no point is placed on the diagonal. The composition of the surface nearly never equals the composition of the reaction medium.

We define the partition coefficient of each ligand at the steady state

$$P_{ligand} = \frac{\text{proportion of ligand in the grafted shell}}{\text{concentration of ligand in solution}} \quad (6)$$

For the exchange of DDT by ligand B, one can define the partition ratio R_B

$$R_B = \frac{P_B}{P_{DDT}} = \frac{\sigma(B)[DDT]_{solution}}{\sigma(DDT)[B]_{solution}} \quad (7)$$

where $\sigma(B)$ and σ(DDT) are the proportions of B and DDT at the surface, respectively. $\%B_{surface}$ can then be expressed as a function of $\%B_{medium}$ using R_B as a parameter (not shown). Note that in the case of equilibrium between the surface and the solution, R_B coincides with the equilibrium constant of Equation (3), as already derived from competitive Langmuir isotherms.[24] Fitting the experimental data (Figure 5a) yields R_B values for the different systems. The scale of partition ratios R_B provides a measurement of the ability for each ligand to exchange DDT ligands (Figure 5b). As expected, the nature of the chain impacts the exchange. For nanoparticles of 5-nm diameter, the more aromatic groups, the higher the affinity for the surface: $R_{TerPh} > R_{BiPh} > R_{Ph}$. This finding is consistent with previous observations, which evidenced the role of the alkylthiol chain length on the exchange, namely a stabilization of the ligand shell for longer chains that yield increased interchain interaction.[38] The origin of this behavior is discussed in details below.

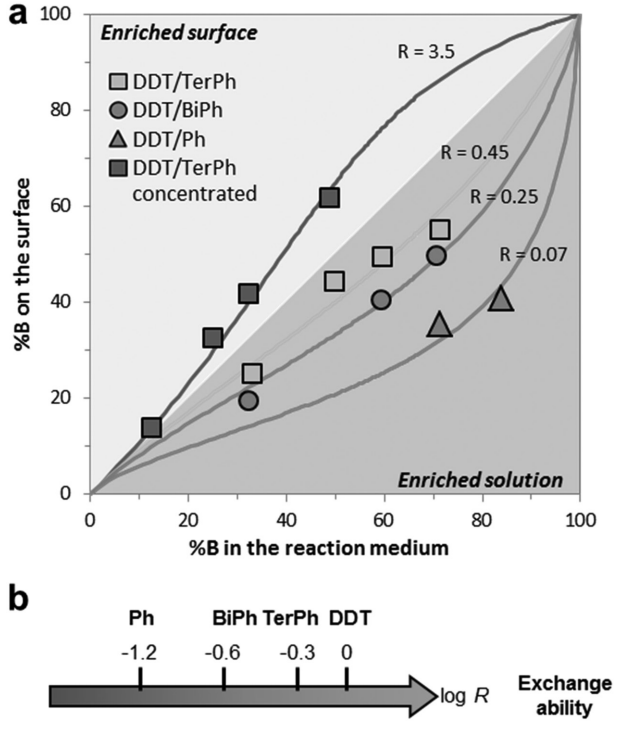

Figure 5. a) Partition of B ligands (TerPh, BiPh, and Ph) on 5-nm nanoparticles for different DDT/B ligands couples in chloroform at particle concentrations of 3×10^{-7} M and also 10^{-4} M for TerPh. b) Exchange ability scale of Ph, BiPh, and TerPh ligands versus DDT in 3×10^{-7} M $CDCl_3$ suspensions.

2.3. Role of the Ligand Functionality on the Exchange: Deciphering the Arylthiols Series by DFT Calculations

Figure 5 shows that TerPh, BiPh, and Ph do not have the same capacity to displace DDT, with binding efficiencies against DDT in the order of TerPh > BiPh >Ph. Modifying the chain may impact ligand binding by changing intermolecular interactions in the SAM, the gold–sulfur interaction through, e.g., electron-donation/withdrawal, and entropic effects. Each phenomenon is considered below as the potential origin of the differences in exchange ability.

2.3.1. Entropy Balance in the Arylthiols Series

In the process of ligand exchange, entropy may impact 1) the free energy of the final DDT/TerPh SAM versus the initial SAM, but also 2) the free energy of solubilized ligands in the surrounding solvent. In the first case, Stellacci and coworkers[16,17,19,41–43] showed that energetically different distributions of the ligands at the surface differ mostly by their entropy. Especially, stabilization of the mixed SAM versus the pure (initial) SAM can occur by entropic effects. Arylthiols have been shown to be relatively homogeneously distributed in a mixed alkyl/arylthiols SAM on 5-nm particles,[41–43] so that configurational entropy (mixing entropy)[16,17,19,41–44] is similar for TerPh, BiPh, and Ph, and does not discriminate these systems. Stabilization of mixed SAMs by conformational entropy (interface entropy originating from the free volume available for the longest ligand chains next to shorter ligands)[16,17,19,41–44] at the interface between two ligands has also been demonstrated. This contribution is negligible for two ligands of similar length (as in the DDT/TerPh system, molecular lengths of ≈1.8 and 1.7 nm for DDT and TerPh,[56] respectively), but increases with the difference in length between both ligands. It has been observed on 5-nm nanoparticles for arylthiols[42,43] and supported by calculations on other systems.[19,41] This effect should stabilize the mixed SAMs in the order TerPh < BiPh < Ph, in opposition to experimental results (Figure 5). In the second case related to the solubilized ligands, upon the 1:1 ligand exchange, the incoming arylthiol ligand loses entropy in the SAM, while the DDT molecule released in the solvent gains entropy. For

molecules TerPh, BiPh, and Ph with similar rigidity, in a given solvent and with a given particle size, the entropic balance during the exchange should be similar and cannot account for the different surface affinities. In the following part, we address the two other potential origins (gold–sulfur bond strength and intermolecular interactions) by comparing the experimental results (Figure 5) with DFT calculations on models of SAMs on flat Au(111) substrates for each DDT/arylthiol couple.

2.3.2. Model SAMs

The DDT SAM was constructed according to a common model (Figure S7 and details in the Supporting Information). For arylthiols, different SAMs configurations are expected to be stable, depending on the experimental conditions:[56,57] the parallel adsorption geometry via π–π interactions on unreconstructed gold or the paired adsorption via σ–π interactions on surface gold adatoms ("T-shaped"). From DFT calculations (not shown for the parallel configuration), the T-shaped configuration is slightly more stable at the same TerPh coverage. We then opted for the latter configuration (**Figure 6**a and details in the Supporting Information), in agreement with previous scanning tunneling microscopy observations on flat Au(111) surfaces.[56]

The adsorption energy of one thiol chain (ΔE_{ads}) in a perfectly ordered SAM is the sum of the binding energy from the sulfur–gold bond $\Delta E_{bind(S-Au)}$ and the intermolecular interactions $\Delta E_{int.chain}$ (including dispersion (London) interactions) between the molecules forming the SAM

$$\Delta E_{ads} = \Delta E_{bind(S-Au)} + \Delta E_{int.chain} \quad (8)$$

ΔE_{ads} and $\Delta E_{bind(S-Au)}$ were evaluated independently by DFT calculations, in order to retrieve $\Delta E_{int.chain}$ (details in the Experimental Section). Briefly, ΔE_{ads} was calculated as the difference between the electronic energy of the SAM and the electronic energies of the free components (thiyl radicals and Au(111) substrate), to which was added the dispersion interaction energy calculated by using a semiempirical dispersion potential with a DFT approach.[58] $\Delta E_{bind(S-Au)}$ was evaluated by a similar approach on a highly diluted SAM. Figure 6b shows the adsorption energies for pure DDT, TerPh, BiPh, and Ph SAMs calculated with (Perdew-Burke-Ernzerhof PBE-D3) and without (PBE) dispersion interactions. The adsorption energy at the PBE-D3 level was also calculated for a mixed DDT/TerPh SAM in a 1/1 ratio (Figure 6b). At the pure PBE level for arylthiols, the intermolecular interactions are calculated to be repulsive. This incorrect result stems from the omission of stabilizing dispersion intermolecular interactions in the assembly at the PBE calculation level. In order to correct this point, we have

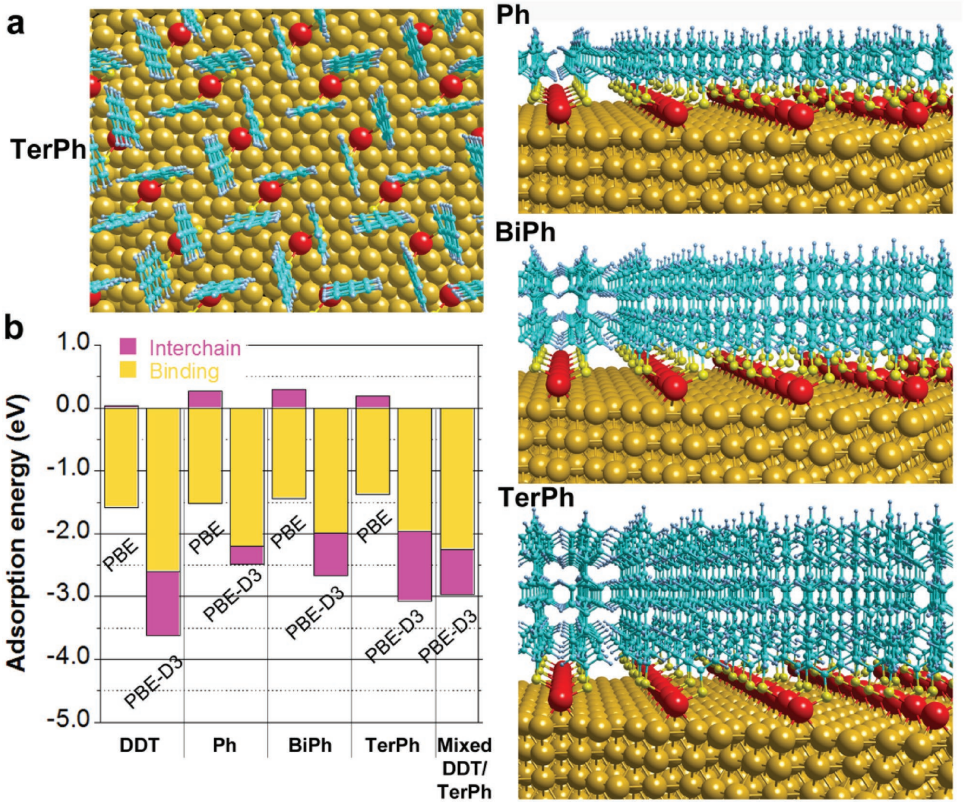

Figure 6. a) Top view of the SAM model for TerPh thiols. Bright yellow: S atoms; blue: C atoms; white: H atoms; dark yellow: gold atoms of the bulk substrate; red: gold adatoms formed by the chemisorption of the arylthiols. On the right: Side views for Ph, BiPh, and TerPh on Au(111). b) Adsorption energies for DDT, Ph, BiPh, TerPh, and mixed DDT:TerPh (1:1) SAMs on Au(111) and the contributions of intermolecular interactions and Au—S bond (binding).

performed calculations at a more advanced level, by taking into account dispersion interactions, of prime importance when interactions between aromatic groups or alkyl chains are at play. This refinement does not impact significantly the Au–S binding energy binding trend, i.e., almost constant within the arylthiol series (±–2.10 eV), but the contribution of intermolecular interactions is radically modified and becomes attractive, as expected. This result validates our procedure for taking into account dispersion interactions.[59]

2.3.3. Impact of the Side Chain on the Gold–Sulfur Interaction

The Au–S bond strength (Figure 6b PBE-D3) is similar within the series of arylthiols studied (about –2.10 eV), whereas for DDT it is equal to –2.60 eV, thus suggesting that changes in the Au–S bond are dependent on the hybridization of the R–C–S carbon atom. Nevertheless, as far as the series of thiols studied here is concerned, the differences in binding energy (max. 0.50 eV) are smaller than the contribution of the dispersion interactions (between –1.1 and –1.94 eV), and thus can be considered to play only a secondary role in the differences in surface affinities of the various ligands.

2.3.4. Intermolecular Interactions: Dispersion Interactions between Arylthiols

The results and discussions above show that the Au–S bond and entropic effects are not the main origin of the differences in the exchange ability of arylthiols (Figure 5). Then, intermolecular interactions should be scrutinized. DFT calculations (Figure 6b), by taking into account dispersion forces, show that attractive intermolecular interactions increase monotonously with the number of phenyl groups in the side chain, as expected from C–H/π (for close to perpendicular phenyl groups in the T-shaped configuration) and π/π (π stacking for parallel phenyl groups) interactions.[58,60] Hence, as observed on planar SAMs,[61] intermolecular interactions between aromatic groups stabilize the final SAM on the surface of the nanoparticles and account for the exchange ability order between arylthiols: $R_{Ph} < R_{BiPh} < R_{TerPh}$.

2.4. Role of the Ligand Functionality on the Exchange: Insights in the Dodecanethiol/Arylthiols System by DFT Calculations

At low concentration, $R_{Ph} < R_{BiPh} < R_{TerPh} < 1$ so that DDT exchange by arylthiol is disfavored (surface empoverished in arylthiols). Entropy and intermolecular interactions may again play a role, as discussed below.

2.4.1. Entropy Balance in the DDT/Arylthiol System

As detailed above, configurational and conformational entropies of the final mixed SAM are higher than the initial DDT SAM and should favor the exchange. Likewise, the entropy balance clearly favors the exchange when a flexible molecule like DDT is released in a good solvent, as chloroform, and replaced in the SAM by a rigid ligand, like TerPh, which does not experience significant entropy loss upon grafting. Both considerations are in opposition to experimental results in the low concentration suspensions, and show that entropy is, again, not the main drive of the exchange.

2.4.2. Intermolecular Interactions: The Role of Dispersion Interactions between Aliphatic Chains in the Alkylthiol DDT SAM

Calculations (Figure 6b) show that the total adsorption energy is higher for DDT than for TerPh because of increased intermolecular interactions. The same holds true for the pure DDT SAM versus the mixed DDT/TerPh SAM (Figure 6b). Dispersion interactions are indeed predominant in a compact fully ordered SAM of long chain alkythiol molecules like DDT.[38,62,63] The adsorption energy order is ΔE_{ads}(DDT) > ΔE_{ads}(TerPh) (absolute values) (Figure 6b). Even by considering a mixed SAM (DDT/TerPh) resulting from the exchange and eventual DDT–TerPh interactions at boundaries (Figure 6b and Figure S8 (Supporting Information)) of potential ligand domains within the mixed SAM, the initial pure DDT SAM is the most stable. This result is in agreement with measured $R_{TerPh} < 1$ for the diluted suspension (Figure 5) and shows again the predominant role of dispersion interactions in exchanges at play in the DDT/arylthiol system.

2.5. Concentration Effect on the Exchange: Insights in the Dodecanethiol/Arylthiol System

For a concentrated suspension and contrary to the low concentration system (Figure 5a), $R_{TerPh} > 1$ on 5-nm nanoparticles, so that DFT calculations do not agree with the experimental observation. According to DFT calculations, fully exchanged and partially exchanged SAMs are close in energy, so that the enthalpy of the final SAM should not change significantly with the composition of the shell.[44] Two other origins may then arise for the increase in R_{TerPh} with the concentration: i) increase in the entropy and stability of the final SAM compared to low concentration, and ii) destabilization of TerPh initially in solution. The first case would be related to changes in the distribution of the ligands in the mixed SAMs upon a change in the concentration. This cause can be ruled out based on previous reports that always show similar stripy or patchy, relatively homogeneous distributions of ligands on 5-nm nanoparticles.[15–17,19,41–43] The second case relates to the solubility of TerPh in chloroform, which may be close to the high concentration investigated ([particle] = 10^{-4} M) and displace Equation (3) toward TerPh binding. This conclusion is supported by the qualitative observation of difficulties to solubilize TerPh in the concentrated system, which requires, e.g., sonication, in opposition to all other ligands studied in the present work. Furthermore, the solvation layer surrounding the bound ligand shell may also impact surface energies, and then relative stabilities of the mixed SAMs.

Because of their similar length, DDT and TerPh should yield similar solvation layers, so that surface energies may not drive the exchange of DDT with TerPh.[14] For the other arylthiols, as explained above, relatively homogeneous distributions of ligands are expected on 5-nm nanoparticles for all ligands,[15–17,19,41–43] so that surface energies of the ligand shell should be similar and should not account for the differences in partition ratios for the various ligands. Through solubility effects, the DDT/TerPh system exemplifies how the exchange ability scale developed herein (Figure 5b) applies for a given solvent, here chloroform.

2.6. Curvature Effect: Insights in the Dodecanethiol/Arylthiol System

The influence of the nanoparticles size—in other words, the surface curvature—was assessed for 5-nm and 2-nm nanoparticles (**Figure 7**) obtained with ligand exchange in a concentrated ([particle] = 10^{-4} M) system. R_{TerPh} of 3.5 with 5-nm diameter decreases to 1.9 with 2-nm diameter. DDT exchange by TerPh is then more efficient on bigger nanoparticles. Several effects may contribute to such enhancement. First, the entropy gain from DDT release upon exchange should be maximized for bigger nanoparticles, on which the DDT SAM is expected to be more packed in the outer part of the shell and more organized (lower entropy of the initial SAM). Second, the stability of the final mixed SAM should be increased on bigger 5-nm nanoparticles through entropic and enthalpic (intermolecular interactions) effects. Indeed, an increase in the nanoparticle size may be accompanied by a change from Janus or patchy surface distribution to a more homogeneous organization of the ligands at the surface.[15–17,19,41–43] This evolution is accompanied by configurational and conformational entropic stabilization of the mixed SAM. Besides, for rigid thiols, the decrease in curvature on big particles brings closer the end groups of neighboring molecules. In the case of TerPh ligands, the distance between the aromatic end groups decreases from 1.2 to 0.8 nm for 2-nm and 5-nm nanoparticles, respectively. Accordingly, phenyl–phenyl interactions are maximized on bigger nanoparticles. This "end-proximity" effect of the particle size may be less pronounced in the initial DDT SAMs, as DDT molecules should be sufficiently flexible to allow conformational changes in the outer shell to increase interchain interactions on both small and big particles.

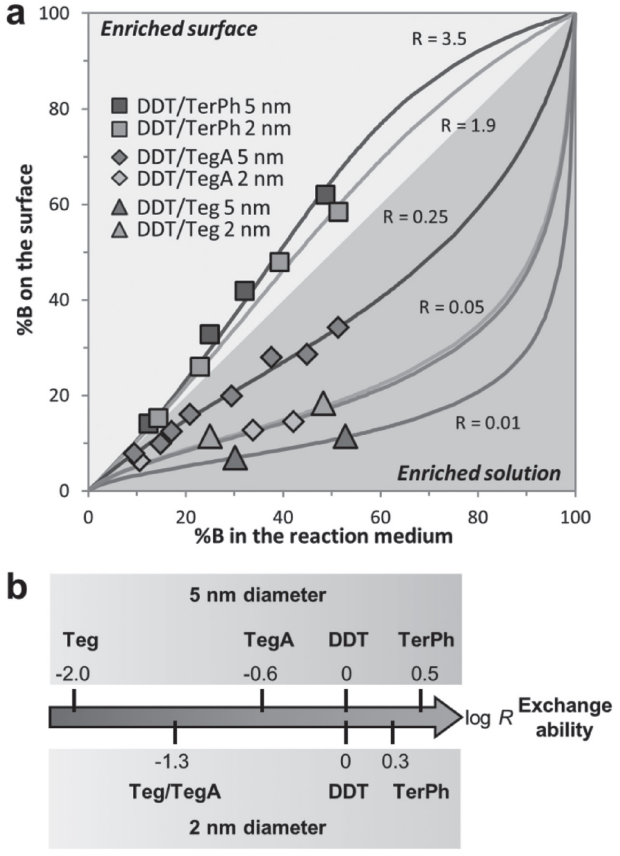

Figure 7. a) Partition of B ligands (TerPh, TegA, and Teg) for [particles] ≈10^{-4} M. Partition ratios *R* are given for each DDT/B couple of ligands. b) Exchange ability scale for TerPh, TegA, and Teg versus DDT at a nanoparticles concentration of ≈10^{-4} M in $CDCl_3$.

2.7. Extended Range of Ligand Functionality by Ligand Exchange

DDT exchange experiments have been extended beyond arylthiols to other ligands ,TegA and Teg (Figures 2 and 7): in concentrated suspensions of 5-nm nanoparticles, $R_{TerPh} > R_{TegA} > R_{Teg}$. In the absence of DFT calculations, only brief, qualitative, and speculative considerations are presented below, to discuss this exchange efficiency order.

Calculations described above (Figure 6) show that the Au–S bond energy is poorly sensitive to strongly conjugated systems. Then, we speculate that the Au–S bond energy is independent of the TegA and Teg substituents, and should not modify the exchange ability.

Based on previous reports,[15–17,19,41–43] one can assume on 5-nm nanoparticles relatively homogeneous (small patches or stripes, not Janus particles) distributions in the mixed SAMs for all ligands, so that mixing entropy is expected to be similar for the DDT/TerPh, DDT/TegA, and DDT/Teg SAMs. As for TerPh, Teg molecules have a length similar to DDT, while TegA is longer than DDT. The gain in conformational entropy during the exchange is then negligible for Teg, but may be large for TegA. The gain in entropy during exchange due to DDT release in the solution accompanying grafting of an incoming ligand is expected to be lower for TegA and Teg that have rigidity similar to DDT than for more rigid TerPh molecules. In brief, entropic effects are expected to favor exchange of DDT with TegA, rather than Teg.

Teg and TegA ethylene glycol units do not form ordered domains[64] because of the competition between dispersion forces, directional interactions between C–O dipoles, and steric repulsion between chains.[65] In the patchy or stripy distributions expected in mixed SAMs on 5-nm nanoparticles,[15–17,19,41–43] TegA molecules can interact together by H-bonds between the amide groups within an SAM, as already demonstrated.[66–68] Therefore, enthalpic stabilization is expected higher for the final mixed SAMs containing TegA

rather than Teg. All in all, both entropic and enthalpic effects favor DDT exchange by TegA, rather than by Teg, in agreement with experiment results (Figure 7).

The nanoparticles size again influences the exchange (Figure 7). Indeed, as for TerPh, exchange by TegA is favored for larger particles. This may again be related to i) the entropy gain during DDT release from a nSAM denser on bigger particles, (i) entropic stabilization of the mixed SAM due to a change in the distribution of the ligands, and (ii) H-bonds more prone to form in a denser SAM on bigger particles. On the contrary, exchange by Teg is disfavored on big particles. Because of similar size and stiffness of the DDT and Teg molecules, entropy gain from solubilized molecules during exchange could be neglected, as well as entropic stabilization of the mixed SAM due to a change in the ligand distribution as the particle size decreases. Thus, a speculative explanation may rely on enthalpic effects: as explained above, incorporating Teg molecules should disturb the densely packed DDT SAM and result in a loss of stabilizing DDT/DDT interactions. Obviously, the discussion drawn in this section requires confirmation by further calculations, out of the scope of this work.

2.8. Effect of the Functionalization Method on the Surface Composition

Finally, NMR titrations have been performed on suspensions of nanoparticles synthesized directly in the presence of ligands couples DDT/TegA and DDT/Teg (biligand syntheses) (**Figure 8**). This method was applied to nanoparticles synthesized through Brust–Schiffrin's and Stucky's protocols in a large range of ligand ratio. Polydispersity varies upon an increase in the proportion of the incoming ligand B (Figures S8–S10, Supporting Information). For the DDT/Teg couple, surface compositions are similar to those measured for ligand exchange (Figure 4). For DDT/TegA, the biligand synthesis leads to a different outcome: the surface is enriched in TegA compared to the synthesis medium, contrary to ligand exchange. Further investigations are required to decipher the different origins of such behaviors (solvation and kinetic effects, for instance).

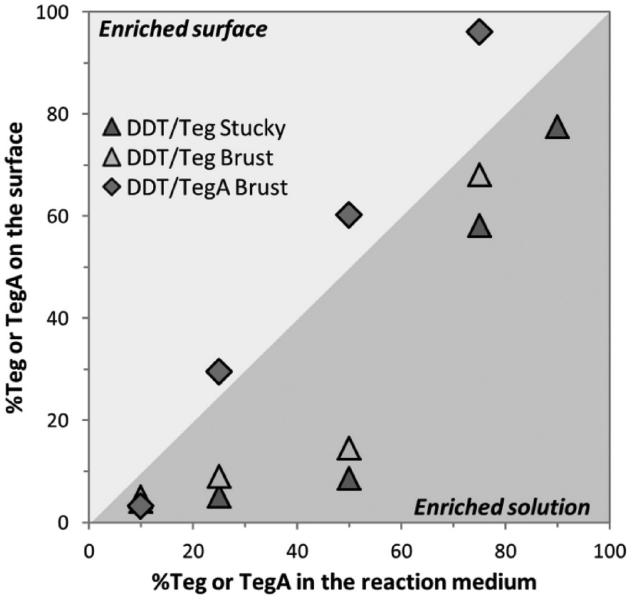

Figure 8. Surface composition versus reaction medium composition for biligand synthesis with different ligand couples and synthesis protocols.

3. Conclusion

The formation of biligand SAMs on gold metal nanoparticles has been monitored by liquid state ^{1}H NMR spectroscopy. The approach allows studying the time evolution of the ligand shell during ligand exchange, up to the steady state, where compositions of the ligand monolayer and the surrounding medium can be quantified after ligand exchange. The resulting molecular partition can be used to build scales of exchange ability for a given initial SAM (an alkylthiol is used herein as a reference) and a specific solvent. Such scales may be used as tools to select the right experimental conditions to target specific surface compositions.

More important, placing different ligands on these scales enables identifying the role of ligand functionality, concentration, and particle size on the exchange. These data shed a new light on the parameters driving the composition of ligand shells: besides the grafting group, the end-group, and the chain length, which have already been studied,[38,39] the nature of the chain also has a large impact on the exchange and the final SAM composition. This approach has been used on the specific case of arylthiol series with the support of DFT calculations. Hence, the role of entropic and intermolecular forces has been deciphered. We have demonstrated that for arylthiols in diluted suspensions, intermolecular forces are the main driving force of the exchange and the origin for the exchange ability varying among the ligand series.

Our experimental results suggest that similar considerations may apply also to other syntheses of multifunctional nanoparticles, such as biligand synthesis, and to other ligands containing polyethylene oxide moieties that are relevant for biological applications.[69–71] In these cases, entropy may play a stronger role, both related to the stability of the final SAM through the surface distribution of the ligands in the mixed SAM,[14,16,17,19,41–43] and to the entropy balance during ligand exchange. Besides, in this article, the reaction pathway for ligand exchange has not been examined. In the future, further calculations may unravel such dynamical effects.

Finally, the methodology developed herein on gold nanoparticles and thiol ligands may be applicable to other kinds of nonmagnetic particles, such as metals and chalcogenides,[37] provided that the ligands can be fully detached from the inorganic core, for instance, with cyanide[25] or aqua regia.[72] The results reported in this study thus pave the way to a rational design of hybrid nanosystems with quantified multifunctionalities.

4. Experimental Section

All reagents were purchased from Sigma-Aldrich and used as received. Details of ligand synthesis, characterization, and DFT calculations are given in the Supporting Information.

Nanoparticle Syntheses: 5-nm gold nanoparticles were synthesized using a method described by Stucky and co-workers.[7] Briefly, $AuCl(PPh)_3$ (300 mg, 1 eq.) was dissolved in 60 mL of toluene with 1.16 mL of DDT (8 eq.). The solution was stirred at 100 °C for 5 min and a preheated solution containing 526 mg (10 eq.) of a *tert*-butylamine borane complex in 36 mL of toluene was added. The mixture was stirred at 100 °C for 3 min and cooled down to room temperature. The gold nanoparticles were precipitated with ethanol and separated from the reaction medium by centrifugation, the supernatant was removed and four cycles of redispersion in toluene (1 mL), precipitation with ethanol (20 mL) and centrifugation were achieved. Then, the particles were dispersed in 80 mL of toluene, the suspension was divided into 5 mL batches, and dried under vacuum.

2-nm gold nanoparticles were synthesized using Brust–Schiffrin's method.[5] 100 mg (1.0 eq.) of $HAuCl_4{\cdot}3H_2O$ was dissolved in 7.5 mL of water and transferred in toluene with a solution of 308 mg of tetraoctylammonium bromide (2.2 eq.) in 5.7 mL of toluene. The aqueous layer was removed and a solution of 51.4 mg (1.0 eq.) of DDT in 1.75 mL of toluene was added. The mixture was stirred and cooled at 0 °C and 7 mL of a cold $NaBH_4$ aqueous solution (0.36 m, 10.0 eq.) was added quickly under vigorous stirring. After 3 h at room temperature the aqueous layer was removed, the organic layer was washed with water, and the particles were precipitated with ethanol and recovered by centrifugation. The washing procedure and fractionation into batches were the same as for the 5-nm particles. Quantitative yields were verified by adding some strong reductant $NaBH_4$ to the colorless supernatants after the first centrifugation. The supernatants remained colorless, thus showing that all gold precursors had reacted.

Biligand Syntheses: The Brust–Schiffrin's protocol remained the same as described above, but DDT was replaced with a mixture of two ligands. Stucky's method for DDT/Teg couple was performed in chloroform at 60 °C for 25 min. For each sample, the washing procedure was modified according to the dispersion ability of the particles. For both methods, the biligand nanoparticles were around 3 nm in diameter (see the Supporting Information). Quantitative yields were verified by the procedure described above.

Ligand Exchange Kinetics: The exchange was performed at 25 °C. A batch of DDT-stabilized gold nanoparticles was dispersed in an NMR tube using $CDCl_3$ to obtain a fresh and stable colloidal dispersion. The ^1H spectrum was acquired. Then, a given quantity of the second ligand was added in a small volume of $CDCl_3$. The mixture was vigorously stirred outside the spectrometer before measurement, and its ^1H spectrum was monitored regularly until it did not change anymore. Every ligand exchange was followed through specific signals, which were deconvoluted if required, e.g., for the DDT/TegA couple. In some cases, little oxidation of the thiols into disulfides occurred. Disulfides could be easily identified by ^1H NMR. With TegA and Teg, a small proportion of disulfides (5–10 mol%) was already present when adding the ligands in the NMR tubes. This quantity sometimes increased, but the conversion of thiols into disulfides occurred after the stabilization of the ligand shell composition. Accordingly, disulfides were considered as not being involved in ligand exchange, in agreement with previous works which had shown that disulfides are much less active than the corresponding thiols in exchange reactions.[38] To assess the effect of concentration, ligand exchange experiments were run with TerPh, BiPh, and Ph ligands, with suspensions initially diluted ≈300 times. Once the steady state was reached, as evidenced by stable UV–vis spectra,[15] the suspensions were concentrated by evaporation in ≈30 min, the particles were washed with ethanol three times to get rid of the free ligands, dried under vacuum, and transferred into NMR tubes with $CDCl_3$ in order to record their ^1H NMR spectra and check for the absence of free ligands. The composition of the ligands shell was then determined by ^1H NMR with the iodine death reaction.[54]

Determination of the Medium and Shell Compositions for Biligand Syntheses: ^1H NMR was again used to assess the composition of the ligand shell after nanoparticles separation and redispersion in $CDCl_3$. A ^1H spectrum was first acquired to quantify the possible remaining free species, then the iodine death reaction[54] was conducted to oxidize all the thiols and recover them as free disulfides in the reaction medium, to be titrated by ^1H NMR.

Supporting Information

Supporting Information is available from the Wiley Online Library or from the author.

Acknowledgements

This work was funded by the C'Nano Ile de France DIM Nano-K under the project NaJaH. L.F.P. and P.Q. thank the support given by the Santa Fe Science Technology and Innovation Agency (ASACTEI, grant 00010-18-2014), CONICET, and PICT-2014-1084.

[1] K. Saha, S. S. Agasti, C. Kim, X. Li, V. M. Rotello, *Chem. Rev.* **2012**, *112*, 2739.
[2] L. Dykman, N. Khlebtsov, *Chem. Soc. Rev.* **2012**, *41*, 2256.
[3] E. C. Dreaden, A. M. Alkilany, X. Huang, C. J. Murphy, M. A. El-Sayed, *Chem. Soc. Rev.* **2012**, *41*, 2740.
[4] M. Montalti, L. Prodi, N. Zaccheroni, R. Baxter, G. Teobaldi, F. Zerbetto, *Langmuir* **2003**, *19*, 5172.
[5] M. Brust, M. Walker, D. Bethell, D. J. Schiffrin, R. Whyman, *J. Chem. Soc., Chem. Commun.* **1994**, 801.
[6] H. Hiramatsu, *Chem. Mater.* **2004**, *16*, 2509.
[7] N. Zheng, J. Fan, G. D. Stucky, *J. Am. Chem. Soc.* **2006**, *128*, 6550.
[8] E. Boisselier, L. Salmon, J. Ruiz, D. Astruc, *Chem. Commun.* **2008**, 5788.
[9] B. C. Mei, K. Susumu, I. L. Medintz, J. B. Delehanty, T. J. Mountziaris, H. Mattoussi, *J. Mater. Chem.* **2008**, *18*, 4949.
[10] A. Verma, O. Uzun, Y. Hu, Y. Hu, H.-S. Han, N. Watson, S. Chen, D. J. Irvine, F. Stellacci, *Nat. Mater.* **2008**, *7*, 588.
[11] C. Vilain, F. Goettmann, A. Moores, P. Le Floch, C. Sanchez, *J. Mater. Chem.* **2007**, *17*, 3509.
[12] A. Ghosh, S. Basak, B. H. Wunsch, R. Kumar, F. Stellacci, *Angew. Chem., Int. Ed.* **2011**, *50*, 7900.
[13] D. Nykypanchuk, M. M. Maye, D. van der Lelie, O. Gang, *Nature* **2008**, *451*, 549.
[14] A. M. Jackson, J. W. Myerson, F. Stellacci, *Nat. Mater.* **2004**, *3*, 330.
[15] C. Goldmann, R. Lazzari, X. Paquez, C. Boissière, F. Ribot, C. Sanchez, C. Chanéac, D. Portehault, *ACS Nano* **2015**, *9*, 7572.
[16] Q. K. Ong, J. Reguera, P. J. Silva, M. Moglianetti, K. Harkness, M. Longobardi, K. S. Mali, C. Renner, S. De Feyter, F. Stellacci, *ACS Nano* **2013**, *7*, 8529.

[17] M. Moglianetti, Q. K. Ong, J. Reguera, K. M. Harkness, M. Mameli, A. Radulescu, J. Kohlbrecher, C. Jud, D. I. Svergun, F. Stellacci, *Chem. Sci.* **2014**, *5*, 1232.
[18] S. Carenco, X. F. Le Goff, J. Shi, L. Roiban, O. Ersen, C. Boissière, C. Sanchez, N. Mézailles, *Chem. Mater.* **2011**, *23*, 2270.
[19] C. Singh, P. Ghorai, M. Horsch, A. Jackson, R. Larson, F. Stellacci, S. Glotzer, *Phys. Rev. Lett.* **2007**, *99*, 226106.
[20] K. M. Harkness, B. C. Hixson, L. S. Fenn, B. N. Turner, A. C. Rape, C. A. Simpson, B. J. Huffman, T. C. Okoli, J. A. McLean, D. E. Cliffel, *Anal. Chem.* **2010**, *82*, 9268.
[21] A. P. Gies, D. M. Hercules, A. E. Gerdon, D. E. Cliffel, *J. Am. Chem. Soc.* **2007**, *129*, 1095.
[22] P. Ionita, A. Caragheorgheopol, B. C. Gilbert, V. Chechik, *J. Am. Chem. Soc.* **2002**, *124*, 9048.
[23] L. Maus, J. P. Spatz, R. Fiammengo, *Langmuir* **2009**, *25*, 7910.
[24] A. Stewart, S. Zheng, M. R. McCourt, S. E. J. Bell, *ACS Nano* **2012**, *6*, 3718.
[25] X. Liu, M. Yu, H. Kim, M. Mameli, F. Stellacci, *Nat. Commun.* **2012**, *3*, 1182.
[26] L. Pasquato, M. Sologan, C. Cantarutti, S. Bidoggia, S. Polizzi, P. Pengo, *Faraday Discuss.* **2016**, *191*, 527.
[27] I. Moreels, B. Fritzinger, J. C. Martins, Z. Hens, *J. Am. Chem. Soc.* **2008**, *130*, 15081.
[28] A. M. Smith, L. E. Marbella, K. A. Johnston, M. J. Hartmann, S. E. Crawford, L. M. Kozycz, D. S. Seferos, J. E. Millstone, *Anal. Chem.* **2015**, *87*, 2771.
[29] L. E. Marbella, J. E. Millstone, *Chem. Mater.* **2015**, *27*, 2721.
[30] G. Guarino, F. Rastrelli, F. Mancin, *Chem. Commun.* **2012**, *48*, 1523.
[31] G. Guarino, F. Rastrelli, P. Scrimin, F. Mancin, *J. Am. Chem. Soc.* **2012**, *134*, 7200.
[32] M. Sologan, D. Marson, S. Polizzi, P. Pengo, S. Boccardo, S. Pricl, P. Posocco, L. Pasquato, *ACS Nano* **2016**, *10*, 9316.
[33] I. Moreels, Y. Justo, B. De Geyter, K. Haustraete, J. C. Martins, Z. Hens, *ACS Nano* **2012**, *5*, 2004.
[34] R. Sharma, G. P. Holland, V. C. Solomon, H. Zimmermann, S. Schiffenhaus, S. A. Amin, D. A. Buttry, J. L. Yarger, *J. Phys. Chem. C* **2009**, *113*, 16387.
[35] R. L. Donkers, Y. Song, R. W. Murray, *Langmuir* **2004**, *20*, 4703.
[36] R. Guo, Y. Song, G. Wang, R. W. Murray, *J. Am. Chem. Soc.* **2005**, *127*, 2752.
[37] R. R. Knauf, J. C. Lennox, J. L. Dempsey, *Chem. Mater.* **2016**, *28*, 4762.
[38] M. J. Hostetler, A. C. Templeton, R. W. Murray, C. Hill, N. Carolina, *Langmuir* **1999**, *15*, 3782.
[39] P. Ionita, A. Caragheorgheopol, B. C. Gilbert, V. Chechik, *J. Am. Chem. Soc.* **2002**, *124*, 9048.
[40] K. Heister, D. L. Allara, K. Bahnck, S. Frey, M. Zharnikov, M. Grunze, *Langmuir* **1999**, *15*, 5440.
[41] P. K. Ghorai, S. C. Glotzer, *J. Phys. Chem. C* **2010**, *114*, 19182.
[42] X. Liu, M. Yu, H. Kim, M. Mameli, F. Stellacci, *Nat. Commun.* **2012**, *3*, 1182.
[43] H. Kim, R. P. Carney, J. Reguera, Q. K. Ong, X. Liu, F. Stellacci, *Adv. Mater.* **2012**, *24*, 3857.
[44] X. Ge, P. C. Ke, T. P. Davis, F. Ding, *Small* **2015**, *11*, 4894.
[45] C. D. Bain, G. M. Whitesides, *J. Am. Chem. Soc.* **1988**, *110*, 6560.
[46] F. Tielens, V. Humblot, C. M. Pradier, M. Calatayud, F. Illas, *Langmuir* **2009**, *25*, 9980.
[47] I. C. Pons-Siepermann, S. C. Glotzer, *ACS Nano* **2012**, *6*, 3919.
[48] Z. Huang, C. Lu, B. Dong, G. Xu, C. Ji, K. Zhao, L.-T. Yan, *Nanoscale* **2016**, *8*, 1024.
[49] J. J. Kuna, K. Voïtchovsky, C. Singh, H. Jiang, S. Mwenifumbo, P. K. Ghorai, M. M. Stevens, S. C. Glotzer, F. Stellacci, *Nat. Mater.* **2009**, *8*, 837.
[50] A. Badia, L. Demers, L. Dickinson, F. G. Morin, R. B. Lennox, L. Reven, *J. Am. Chem. Soc.* **1997**, *119*, 11104.
[51] Z. Hens, J. C. Martins, *Chem. Mater.* **2013**, *25*, 1211.
[52] F. Ribot, V. Escax, C. Roiland, C. Sanchez, J. C. Martins, M. Biesemans, I. Verbruggen, R. Willem, *Chem. Commun.* **2005**, 1019.
[53] O. Kohlmann, W. E. Steinmetz, X. Mao, W. P. Wuelfing, A. C. Templeton, R. W. Murray, C. S. Johnson, *J. Phys. Chem. B* **2001**, *105*, 8801.
[54] A. C. Templeton, M. J. Hostetler, C. T. Kraft, R. W. Murray, *J. Am. Chem. Soc.* **1998**, *120*, 1906.
[55] H. Hinterwirth, S. Kappel, T. Waitz, T. Prohaska, W. Lindner, M. Lämmerhofer, *ACS Nano* **2013**, *7*, 1129.
[56] A. Bashir, W. Azzam, M. Rohwerder, A. Terfort, *Langmuir* **2013**, *29*, 13449.
[57] V. V. Korolkov, S. Allen, C. J. Roberts, S. J. B. Tendler, *J. Phys. Chem. C* **2011**, *115*, 14899.
[58] X. Wu, M. C. Vargas, S. Nayak, V. Lotrich, G. Scoles, *J. Chem. Phys.* **2001**, *115*, 8748.
[59] D. Costa, C.-M. Pradier, F. Tielens, L. Savio, *Surf. Sci. Rep.* **2015**, *70*, 449.
[60] M. Alonso, T. Woller, F. J. Martín-Martínez, J. Contreras-García, P. Geerlings, F. De Proft, *Chem. - Eur. J.* **2014**, *20*, 4931.
[61] E. Sabatani, J. C. Cohen-Boulakia, M. Bruening, I. Rubinstein, *Langmuir* **1993**, *9*, 2974.
[62] W. J. Miller, N. L. Abbott, *Langmuir* **1997**, *13*, 7106.
[63] C. Vericat, M. E. Vela, G. Benitez, P. Carro, R. C. Salvarezza, *Chem. Soc. Rev.* **2010**, *39*, 1805.
[64] P. Harder, M. Grunze, R. Dahint, D. Heidelberg, *J. Phys. Chem. B* **1998**, *5647102*, 426.
[65] R. A. Boto, J. Contreras-García, M. Calatayud, *Comput. Theor. Chem.* **2015**, *1053*, 322.
[66] A. K. Boal, V. M. Rotello, *Langmuir* **2000**, *16*, 9527.
[67] R. S. Clegg, J. E. Hutchison, *J. Am. Chem. Soc.* **1999**, *20*, 5319.
[68] P. M. Donaldson, P. Hamm, *Angew. Chem., Int. Ed.* **2013**, *52*, 634.
[69] A. G. Kanaras, F. S. Kamounah, K. Schaumburg, C. J. Kiely, M. Brust, *Chem. Commun.* **2002**, 2294.
[70] T. A. Larson, P. P. Joshi, K. Sokolov, *ACS Nano* **2012**, *6*, 9182.
[71] F. Schulz, T. Vossmeyer, N. G. Bastús, H. Weller, *Langmuir* **2013**, *29*, 9897.
[72] J. J. Buckley, E. Couderc, M. J. Greaney, J. Munteanu, C. T. Riche, S. E. Bradforth, R. L. Brutchey, *ACS Nano* **2014**, *8*, 2512.

Received: December 3, 2016
Revised: January 30, 2017
Published online:

